Widespread and intense wildfires at the Paleocene-Eocene boundary

M.K. Fung, M.F. Schaller, C.M. Hoff, M.E. Katz, J.D. Wright

Supplementary Information

The Supplementary Information includes:

➢ Materials and Methods
➢ Supplementary Text
➢ Tables S-1 and S-2
➢ Figures S-1 to S-5
➢ Supplementary Information References

Materials and Methods

Samples of ~30-40 g dry weight (where available) were taken below and through the onset of the Paleocene-Eocene boundary carbon isotope excursion at Wilson Lake B (WL; 39.6598 °N, 75.0472 °W) and Randall's Farm (RF; 38.833 °N, 76.799 °W) cores. Sediment samples were soaked in DI water, washed through both 45 and 63 μm sieves, and oven dried at 50 °C overnight. All sediment fines (<45 μm) were saved from both sites.

We use scanning electron microscopy (SEM), Raman spectroscopy, and wavelength-dispersive X-ray spectroscopy (WDS) to identify the nature of the black grains and confirm that they are fossilised charcoal. Secondary electron images of representative charcoal pieces are made on a Zeiss EVO-MA15 scanning electron microscope at Union College in Schenectady, New York. For secondary electron imaging, all charcoal samples are sputter coated in gold-palladium. SEM imaging shows finely preserved plant anatomical features, characteristic of charcoal (Fig. S-2). Unlike charcoal, coal exhibits conchoidal fracture in SEM images (Glasspool and Scott, 2013). Raman spectra are collected using a Bruker SENTERRA Raman microscope with a 532 nm laser at Rensselaer Polytechnic Institute (RPI), are background-corrected, and compared to charcoal and graphite standards, and other maceral groups from Ulyanova *et al.* (2014) (Fig. S-4). WL and RF spectra are nearly identical to the charcoal standard and clearly distinct from the graphite standard. Furthermore, Ulyanova *et al.* (2014) observes a higher wavelength G-band and lower wavelength and narrower D1-band in the more ordered anthracite and coal spectra at 1580-1600 cm^{-1} and 1350-1400 cm^{-1} wavenumbers, respectively (Wang *et al.*, 2014) compared to that of our charcoal. Our Raman results for the WL and RF material best match the charcoal standard. Resolution for Raman measurements is 1-3 cm^{-1}. WDS measurements are made using a Cameca SX-100 electron microprobe at RPI. Measurements of the black grains are done at 15 keV with a beam current of 20 nA with a Ni-C pseudocrystal to measure carbon. Samples were coated in platinum. The average standard deviation for individual carbon measurements is ~1 %. WDS measurements indicate the grains are 58-84 % carbon by weight (average ~74 %). The carbon content of bituminous coal and anthracite ranges from 86-98 %, Ulyanova *et al.* (2014), further supporting the charcoal nature of our material.

To calculate the abundance of charcoal throughout WL and RF, charcoal pieces were isolated through a sink-swim analysis technique where charcoal pieces were floated in a solution of lithium metatungstate (LMT) gravimetrically diluted to a density of

2.2 g/cm³. Individual charcoal grains were counted in the >63 µm size fraction for charcoal abundance and normalised per gram dry sediment. These counts were checked by manual picking of an entire unfloated sample. Samples from this size fraction allow us to observe anatomical plant structure, further ensuring the material is charcoal. We find that our sink-swim technique recovers about 81 % of the charcoal that could be visually identified and separated by manually picking a sample. The $\delta^{13}C_{charcoal}$ is measured at RPI on an Elementar ISOTOPE Select elemental analyser (EA) coupled to an Isoprime 100 isotope ratio mass spectrometer (IRMS) run in continuous flow mode. The NBS22 standard was analysed multiple times in each sample run, with a 2σ analytical error of 0.12 ‰ in the weight range of the charcoal grains. The $\delta^{13}C_{charcoal}$ presented here are made on a random selection of 4-12 µg of ~20 charcoal grains isolated from a single sample. Manually and physically separating the charcoal from the bulk sample ensures that we analyse a consistent carbon-bearing phase through the section.

By individually picking or physically separating charcoal pieces for isotope analysis, as opposed to the bulk processing techniques used in previous studies (Moore and Kurtz, 2008), we ensure that the material we analyse remains consistent throughout the section and also between sites. Furthermore, we confirm that the isotope values we report have been measured on fossil charcoal and not another organic phase.

Reflectance measurements were contracted to Maria Mastalerz at Indiana University, and were made on individual charcoal fragments to infer the temperature of formation. Due to feasibility issues (cost, size, difficulty in polishing), measurements were completed on only 7 fragments from both sites. Petrographic observations and reflectance analyses were carried out in a Leica DM 2500P reflected-light microscope linked to a TIDAS PMT IV photometric system. Maceral groups were identified based on their optical characteristics (morphology, cell structure preservation, reflectance, *etc.*) For maceral reflectance analysis (R_o random), 25 measurements were averaged.

Supplementary Text

Characterising the P-E Charcoal

Charcoal deposition in marine sediments is controlled primarily by fire frequency and secondarily by wind transport of charcoal from land to ocean (Herring, 1985), with more wildfire activity resulting in higher charcoal flux to marine sediments. At both WL and RF, the anomalous abundance of fossilised charcoal that occurs above the P-E spherule layer indicates that increased wildfire activity followed the extraterrestrial impact. Direct comparison of our charcoal abundance data to other shallow-marine deposits is challenging, because of the scarcity of methodological studies on lower Tertiary charcoalified plant deposits (Scott, 2000). For example, studies examining charcoal fluxes into marine sediments during the Cenozoic measured charcoal concentrations through bulk extraction techniques on the entire sediment sample (Herring, 1985), in contrast to our charcoal abundance counts which are constrained to the 63-150 µm size fraction. Furthermore, documented charcoal flux rates as old as the P-E boundary are rare (Herring, 1985). This problem is further exacerbated by the lack of systematic standardisation of both identification and analytical quantification of charcoal in different environments (Schmidt and Noack, 2000).

The use of chemical methods to quantify black carbon is most frequently employed, but is not an exact measure of charcoal (Scott, 2010). Graphitic black carbon (GBC) at the farther offshore Bass River Site (ODP 174AX) shows a $\delta^{13}C_{GBC}$ excursion that appears to be coincident with the CIE onset in bulk calcium carbonate (Moore and Kurtz, 2008); however, these results are not comparable to our $\delta^{13}C_{charcoal}$ for several reasons. Moore and Kurtz (2008) use a bulk extraction method to isolate GBC, which can incorporate GBC of different origins along with unrelated organics, leading to a mixed signal from multiple sources. Furthermore, wildfires are not the sole source of GBC (Goldberg, 1985), whereas charcoal on the shelf is exclusively of wildfire origin (Belcher *et al.*, 2003). Our $\delta^{13}C$ measurements were performed only on individual fragments confirmed to be charcoal (see Fig. S-2), thereby eliminating contamination from bulk sedimentary constituents. If the GBC is indeed evidence of wildfires, its coincidence with the CIE onset in bulk carbonate is consistent with a much lower sedimentation rate at the Bass River (BR) site (Stassen *et al.*, 2012). We note that the offset between the CIE in charcoal and the CIE in carbonate is variable and increases with decreasing water depth at WL and RF, where BR may be the offshore end-member.

We note that when plotted by depth, events 1 and 2 on Figure 3 appear further apart at RF than at WL; this is likely an artifact of the much lower sampling resolution and higher sedimentation rate at RF compared to WL and the ~61 cm sampling gap between the sample containing the apparent charcoal peak and the sample immediately below. The larger separation between peaks at RF compared to WL is also consistent with a higher sedimentation rate at the shallower, more proximal (close to shoreline) site (similar to relationships in modern coastal regions (Kuehl *et al.*, 1986)).

We compare our charcoal results to magnetic records using the ratio of saturation remanence to saturation magnetization (M_r/M_s) at WL (Kent *et al.*, 2017) and ferromagnetic resonance spectroscopy (FMR α) at RF (Kopp *et al.*, 2009). These two magnetic parameters are related indicators of single domain magnetite, and M_r/M_s measured elsewhere in the Marlboro Clay at Ancora and

Bass River (Kent *et al.,* 2003) show coincident changes with FMR α (Kopp *et al.,* 2007; 2009). The increase in magnetic nanoparticles near the base of the Marlboro Clay extends even farther than the charcoal record at WL and RF, as documented in sites across the Salisbury Embayment from northern New Jersey to southern Virginia (~400 km) (Kopp *et al.,* 2009; Kent *et al.,* 2003; Lanci *et al.,* 2002), indicating that the wildfires were regionally widespread and synchronous (within the level of resolution possible).

Vegetation that remains dead for a long period of time before burning can exhibit pre-charring biodegradation (Jones and Lim, 2000). None of the charcoal fragments that we imaged display features characteristic of biodegradation, such as perforations and trackways, indicating that there was no significant delay between P-E plant death and conversion to charcoal. This lack of delay does not discount the possibility that the P-E charcoal formed when the remains of plants perished from "ordinary" causes (*i.e.* not the victim of an extraterrestrial impact) and simply died from hotter, dryer climate conditions, and eventually turned into charcoal as the result of intense widespread wildfires ignited by a common method (*e.g.,* lightning).

Linking Wildfires and Extraterrestrial Impacts

Following the Cretaceous-Paleogene boundary (K-Pg) impact event, a global K-Pg soot layer was produced by combustion of large amounts of vegetation in a firestorm ignited by an extraterrestrial impact (Wolbach *et al.,* 1985; 1990a; 1990b; Venkatesan and Dahl, 1989). Thermal radiation and ejecta fallout from the K-Pg impact likely ignited widespread wildfires (Shuvalov, 2001). Impact models demonstrate that the necessary thermal radiation could have originated from: 1) hot, compressed air released by the shockwave; 2) the vapor plume (composed of vaporised impactor and target rock, called the "fireball"); and 3) re-entry and fallout of ejecta sufficient to ignite massive wildfires (Melosh *et al.,* 1990; Collins et al., 2005; Kring and Durda, 2002; Durda and Kring 2004). The occurrence of wildfires is also supported by a "fern spike" (Tschudy *et al.,* 1984), as well as a dramatic increase in fusain (fossil charcoal) following the K-Pg boundary near the impact site (Kruge *et al.,* 1994), although the global nature of fusain deposition has not been established. The lack of above-background charcoal levels in the U.S. Western Interior and abundance of non-charred plant fragments in K-Pg material suggests the wildfires may have been widespread but only regional, although this apparent deficiency of charcoal may have been interpreted due to incorrect sedimentation rates (see Roberston *et al.,* 2013 cf. Belcher *et al.,* 2003 and Scott *et al.,* 2000). Furthermore, Jones and Lim (2000) found evidence of biodegradation in 53 % of charcoal fragments examined from K-Pg sites, suggesting time lag between plant mortality and subsequent burning. Nonetheless, a comparison of our results to the sequence of K-Pg events is beneficial, as we unequivocally show above-background levels of charred plant material (charcoal) at the P-E boundary.

Marlboro Clay

Recently formed charcoal has a density less than water and initially floats (Nichols *et al.,* 2000). The buoyancy of the charcoal grains (which keeps the particles suspended until becoming waterlogged (Vaugh and Nichols, 1995; Rhodes, 1996), compared to the greater density of the clay particles explains why the charcoal peak is slightly above the base of the clay. Major storm events produce fluidised mudflows composed of suspended sediment that are eventually deposited in the inner shelf (Geyer *et al.,* 2000; Goff *et al.,* 2013). Additionally, in modern California, rapidly developed hyperpycnal sediment gravity currents deposit massive amounts of fluidised mud, formed within hours following moderately sized river discharge events (Warrick *et al.,* 2007). Mudflow densities are >2.0 g/cm^3 due to increased sediment load (Woolley, 1946; Sharp and Nobles, 1963). Considerable density stratification occurs due to the excess density of these mudflows (Ross and Mehta, 1989). Therefore, it is possible that the less dense charcoal floated within the mudflows, creating the observed offset in the charcoal abundance and clay boundary level.

We consider Marlboro Clay sedimentation rates and duration for the CIE onset using end-member scenarios (Table S-2) to provide context for our findings. An independent submillennial-scale CIE onset for Site 690 using a cyclostratigraphic age model is also shown for perspective (Röhl *et al.,* 2007). Because there is no agreement on the sedimentation rate of the Marlboro Clay at the CIE onset, it is difficult to provide a timeline for our order of events. Even though our findings cannot provide precise timing for the CIE onset, an important result is that they do not support a millennial onset. Such a timeframe would require no plant growth for thousands of years and a widespread spike in wildfire activity that is temporally unrelated to the onset of the CIE, making its origin ambiguous.

Supplementary Tables

Table S-1 Reflectance measurements (R_o) and corresponding temperature of formation (Scott and Jones, 1991) for samples from WL and RF. Highest R_o values, and inferred formation temperatures come from the charcoal peaks at both RF and WL sites.

| Site	Depth (ft)	Depth (m)	Average Reflectance R_o	Temperature (°C)*
RF	63.5	19.35	1.24	341
RF	65.5	19.96	0.64	267
RF	74.9	22.83	0.76	283
WL	354.9	108.17	0.86	295
WL	365.1	111.28	1.10	324
WL	365.8	111.50	2.99	552
WL	366.6	111.74	0.38	237

Table S-2 Comparison of sedimentation rates and duration of the CIE onset from multiple palaeo-shelf sites and a deep-sea site. Paleodepth ranges for sites are shown.

|	Salisbury Embayment – Marlboro Clay			Deep Sea
Study:	Wright and Schaller (2013)	Self-Trail *et al.* (2017)	Zeebe *et al.* (2016)	Rohl *et al.* (2007)
Site:	Millville and Wilson Lake B (~59 and ~39 m)	Mattawoman Creek-Billingsley Road (MCBR) (~10-30 m)	Millville (~59 m)	Site 690 (1800 m)
Sedimentation Rate:	2 cm yr^{-1}	50 cm kyr^{-1}	6.2 cm kyr^{-1}	1.3 cm kyr^{-1}
CIE Duration:	~13 yr	4 kyr	4 kyr	<750 yr

Supplementary Figures
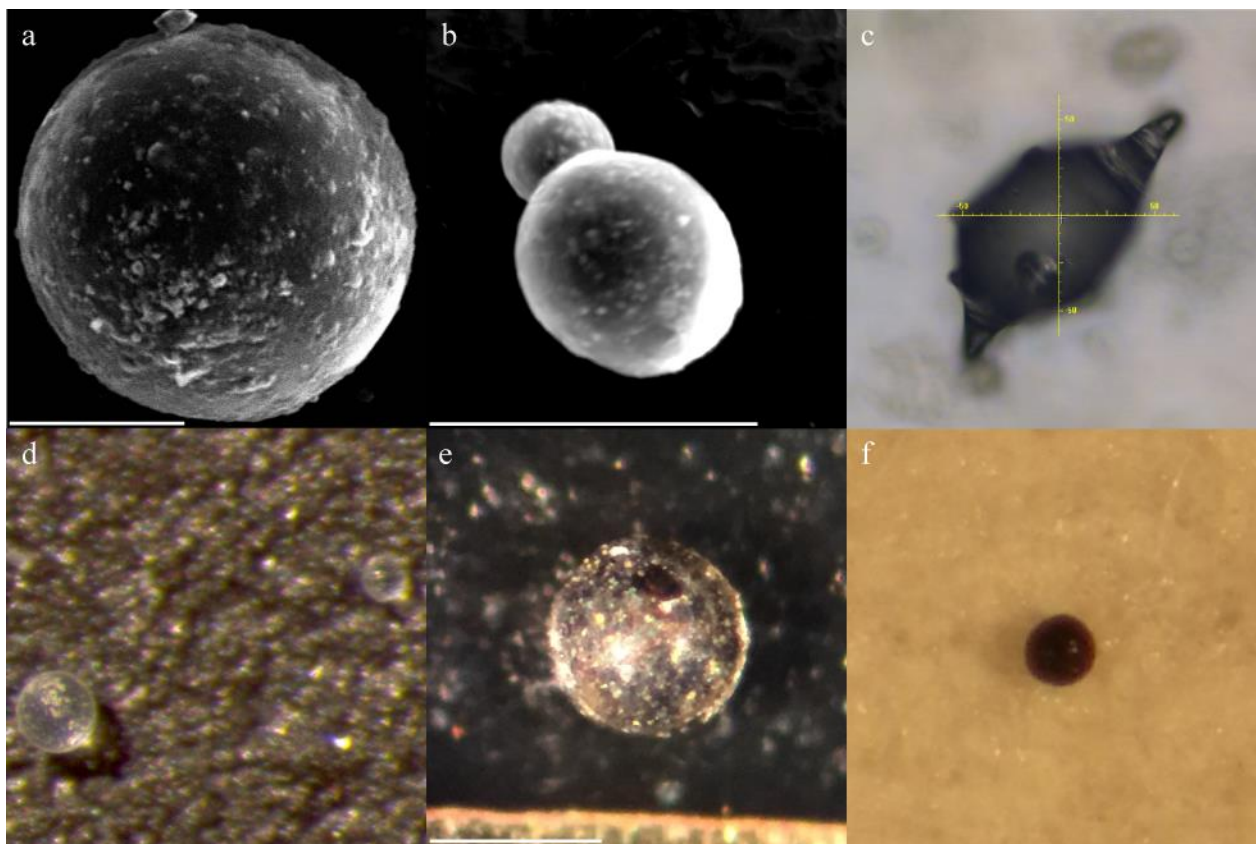
Figure S-1   SEM (a-b) and light micrograph (c-f) images of RF spherules. White scale bar is 50 microns. See Schaller *et al*. (2016) and Schaller and Fung (2018) for detailed physical and chemical descriptions of spherules at other sites. Note, spherules from RF were some of the very first identified and much of the material was expended during the initial characterisation stage. These spherules were imaged prior to using a white picking tray.
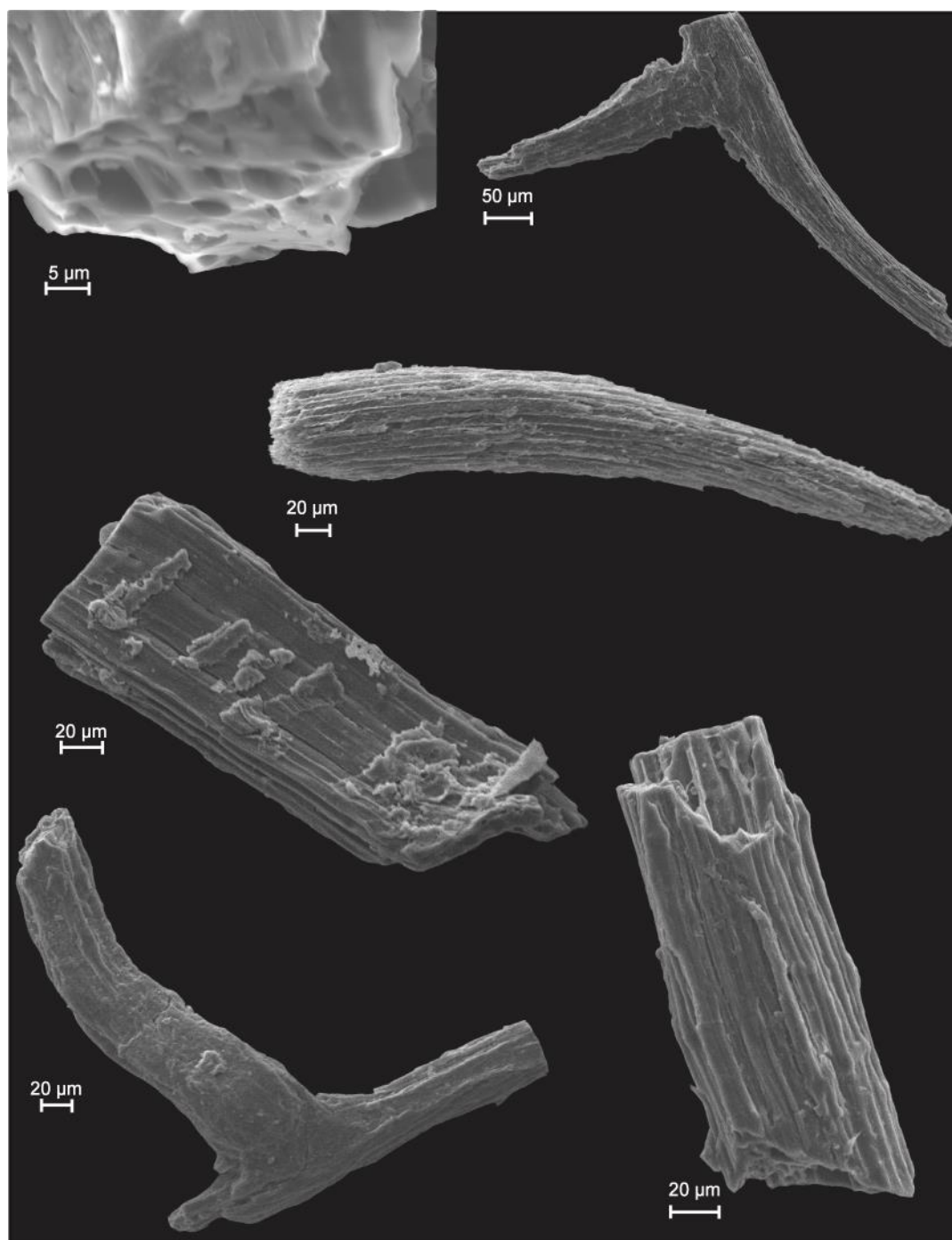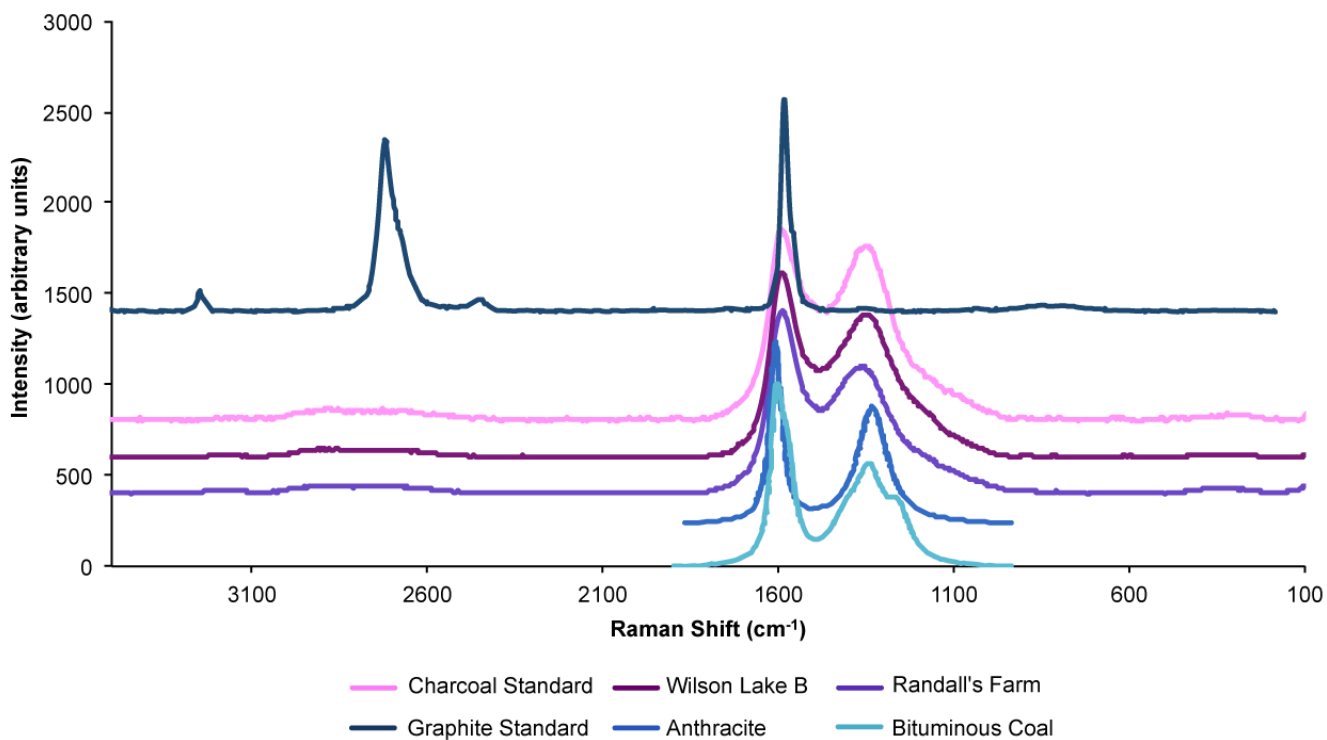
Figure S-2   SEM images of representative charcoal fragments from WL and RF reveal elongate xylem fibers, detailed tracheid cells, smooth homogenised cell walls, and well-preserved internal honeycomb structures. Working distances range from 5-24 mm and EHT is set at 15 kV.

Wilson Lake B
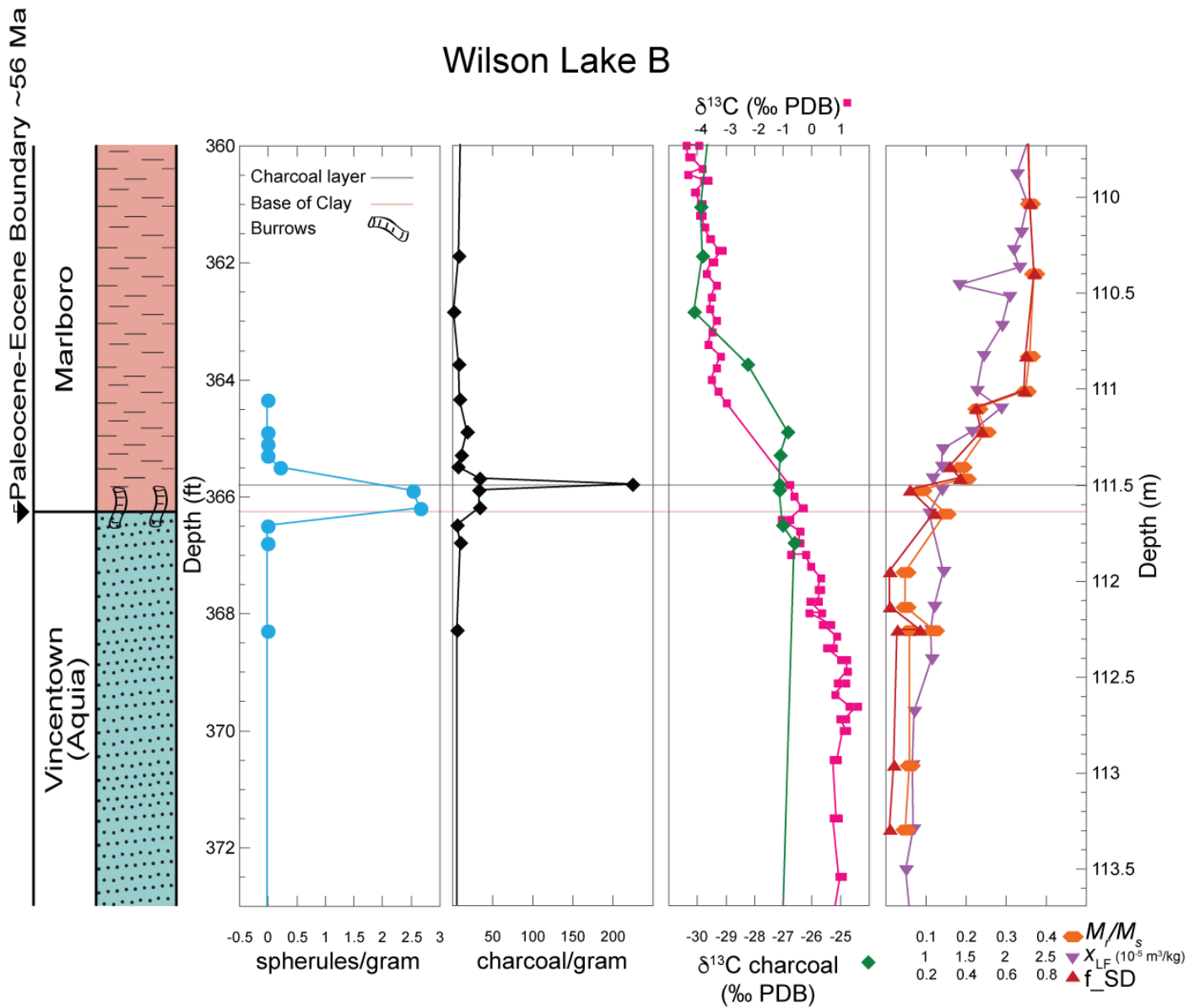
Figure S-3 Expanded CIE onset at WL. Charcoal abundance and $\delta^{13}C_{charcoal}$ plotted with $\delta^{13}C_{bulk}$ and spherules/gram discovered at WL. Ratio of saturation remanence to saturation magnetization (M_r/M_s), low-field magnetic susceptibility (X_{LF}), and volume weighted SD fraction (f_SD) at WL (Kent *et al.,* 2017) illustrates how the abrupt rise in magnetization is coincident with the increase in charcoal abundance.

Figure S-4   Raman spectra of representative charcoal pieces from WL and RF, compared to a wood charcoal standard, graphite (RRUFF IDR050503), anthracite (Ulyanova *et al.,* 2014), and bituminous coal (Ulyanova *et al.,* 2014). Raman spectra from Ulyanova *et al.* (2014) are presented in the 900-1900 cm^{-1} wavenumber range.

Figure S-5   Representative images of polished charcoal fragments from WL and RF. Note smooth, well-preserved cell walls present in the samples. Bright areas are post-depositional pyrite.

Supplementary Information References

Belcher, C.M., Collinson, M.E., Sweet, A.R., Hildebrand, A.R., Scott, A.C. (2003) Fireball passes and nothing burns - The role of thermal radiation in the Cretaceous-Tertiary event: Evidence from the charcoal record of North America. *Geology* 31, 1061-1064.

Collins, G.S., Melosh, H.J., Marcus, R.A. (2005) Earth Impact Effects Program: A Web-based computer program for calculating the regional environmental consequences of a meteoroid impact on Earth. *Meteoritics & Planetary Science* 40, 817-840.

Durda, D.D., Kring, D.A. (2004) Ignition threshold for impact-generated fires. *Journal of Geophysical Research* 109, 1-14.

Geyer, W.R., Hill, P., Milligan, T., Traykovski, P. (2000) The structure of the Eel River plume during foods. *Continental Shelf Research* 20, 2067-2093.

Glasspool, I.J., Scott, A.C. (2013) Identifying Past Fire Events. In: Belcher, C. M. (Eds.) *Fire Phenomena and the Earth System: An Interdisciplinary Guide to the Fire Science*. John Wiley & Sons, Ltd, Chichester, 179-206.

Goff, J.A. et al. (2013) Rapid Response Survey Gauges Sandy's Impact on Seafloor. *EOS* 94(39), 337-348.

Goldberg, E.D. (1985) Black Carbon in the Environment: Properties and Distribution. John Wiley, New York.

Herring. J.R. (1985) Charcoal fluxes into sediments of the North Pacific Ocean: the Cenozoic record of burning. In: Sundquist, E.T., Broecker, W.S. (Eds) The Carbon Cycle and Atmospheric CO2: Natural Variations Archean to Present. *Geophysical Monograph*. 419-442.

Jones, T.P., Lim, B. (2000) Extraterrestrial impacts and wildfires. *Palaeogeography, Palaeoclimatology, Palaeoecology* 164, 57-66.

Kent, D.V., Cramer, B.S., Lanci, L., Wang, D., Wright, J.D., Van der Voo, R. (2003) A case for a comet impact trigger for the Paleocene/Eocene thermal maximum and carbon isotope excursion. *Earth and Planetary Science Letters* 211, 13-26.

Kent, D.V., Lanci, L., Wang, H., Wright, J.D. (2017) Enhanced magnetization of the Marlboro Clay as a product of soil pyrogenesis at the Paleocene-Eocene Boundary? *Earth and Planetary Science Letters* 473, 303-312.

Kring, D.A., Durda, D.D. (2002) Trajectories and distribution of material ejected from the Chicxulub impact crater: Implications for postimpact wildfires. *Journal of Geophysical Research* 107, 6-22.

Kruge, M.A., Stankiewicz, A.B., Crelling, J.C., Montanari, A., Bensley, D.F. (1994) Fossil Charcoal in Cretaceous-Tertiary boundary strata: Evidence for catastrophic firestorm and megawave. *Geochimica et Cosmochimica Acta* 58, 1393-1397.

Kuehl, S.A., DeMaster, D.J., Nittrouer, C.A. (1986) Nature of sediment accumulation on the Amazon continental shelf. *Continental Shelf Research* 6, 209-225.

Lanci, L., Kent, D.V., Miller, K.G. (2002) Detection of Late Cretaceous and Cenozoic sequence boundaries on the Atlantic coastal plain using core log integration of magnetic susceptibility and natural gamma ray measurements at Ancora, New Jersey. *Journal of Geophysical Research* 107, 2216.

Melosh, H.S., Schneider, N.M., Zahnlek, J., Latham, D. (1990) Ignition of global wildfires at the Cretaceous/Tertiary boundary. *Nature* 343, 251-254.

Moore, E.A., Kurtz, A.C. (2008) Black carbon in Paleocene-Eocene boundary sediments: A test of biomass combustion as the PETM trigger. *Palaeogeography, Palaeoclimatology, Palaeoecology* 267, 147-152.

Nichols G.J., Cripps J.A., Collinson M.E., Scott A.C. (2000) Experiments in waterlogging and sedimentology of charcoal: results and implications. *Palaeogeography, Palaeclimatology, Palaeecology* 164, 43-56.

Rhodes, A.N. (1996) Moorland Fire History from Microscopic Charcoal in Soils and Lake Sediments. PhD Thesis. University of Newcastle upon Tyne, 25-26.

Robertson, D.S., Lewis, W.M., Sheehan, P.M., Toon, O.B. (2013) K-Pg extinction: Reevaluation of the heat-fire hypothesis. *Journal of Geophysical Research: Biogeosciences* 118, 329-336.

Röhl, U., Westerhold, T., Bralower, T.J., Zachos, J.C. (2007) On the duration of the Paleocene–Eocene thermal maximum (PETM). *Geochemistry Geophysics Geosystems* 8, 1-13.

Ross M.A., Mehta, A.J. (1989) On the Mechanics of Lutoclines and Fluid Mud. *Journal of Coastal Research* 5, 551-62.

Self-Trail, J. M., et al. (2017) Shallow marine response to global climate change during the Paleocene-Eocene Thermal Maximum, Salisbury Embayment, USA. *Paleoceanography* 32, 710-728.

Schaller, M.F., Fung, M.K., Wright, J.D., Katz, M.E., Kent, D.V. (2016) Evidence of an Extraterrestrial Impact at the Paleocene-Eocene boundary. *Science* 354, 225-229.

Schaller, M.F., Fung, M.K. (2018) The extraterrestrial impact evidence at the Paleocene-Eocene boundary and sequence of environmental change on the continental shelf. *Philosophical Transactions of the Royal Society A* 376, doi: 10.1098/rsta.2017.0081.

Schmidt, M.W., Noack, A.G. (2000) Black carbon in soils and sediments: Analysis, distribution, implications, and current challenges. *Global Biogeochemical Cycles* 14, 777-793.

Scott, A.C. (2000) The Pre-Quaternary history of fire. *Palaeogeography, Palaeoclimatology, Palaeoecology* 164, 281-329.

Scott, A.C. (2010) Charcoal recognition, taphonomy and uses in palaeoenvironmental analysis. *Palaeogeography, Palaeoclimatology, Palaeoecology* 291, 11-39.

Scott, A.C., Jones, T.P. (1991) Microscopic observations of Recent and fossil charcoal. *Microscopy and Analysis* 25, 13-15.

Scott, A.C., Lomax, B.H., Collinson, M.E., Upchurch, G.R., Beerling, D.J. (2000) Fire across the K-T boundary: initial results from the Sugarite Coal, New Mexico, USA. *Palaeogeography, Palaeoclimatology, Palaeoecology* 164, 381-395.

Sharp, R.P., Nobles, L.H. (1963) Mudflow of 1941 at Wrightwood, Southern California. *Bulletin of the Geological Society of America* 64, 547-560.

Shuvalov, V.V. (2001) Radiation effects of the Chicxulub impact event. In: Buffetaut, E., Koeberl, C (Eds) *Geological and biological effects of impact events*. Springer, Berlin, Federal Republic of Germany, 237-247.

Stassen, P., Thomas, E., Speijer, R.P. (2012) The progression of environmental changes during the onset of the Paleocene-Eocene thermal maximum (New Jersey Coastal Plain). *Austrian Journal of Earth Sciences* 105, 169-178.

Tschudy, R.H., Pillmore, C.L., Orth, C.J., Gilmore, J.S., Knight, J.D. (1984) Disruption of the terrestrial plant ecosystem at the Cretaceous-Tertiary boundary, Western Interior. *Science* 225, 1030-1032.

Ulyanova, E.V., Molchanov, A.N., Prokhorov, I.Y., Grinyov, V.G. (2014) Fine structure of Raman spectra in coals of different rank. *International Journal of Coal Geology* 121, 37-43.

Vaughn, A., Nichols, G. (1995) Controls on the deposition of charcoal: implications for sedimentary accumulations of fusain. *Journal of Sedimentary Research* A65(1), 129-135.

Venkatesan, M.I., Dahl, J. (1989) Organic geochemical evidence for global fires at the Cretaceous/Tertiary boundary. *Nature* 338, 57-60.

Wang, S., Cheng, H., Jiang, D., Huang, F., Su, S., Bai, H. (2014) Raman spectroscopy of coal component of Late Permian coals from Southern China. *Spectroscopy* 132, 767-770.

Warrick, J.A., Xu, J., Noble, M.A., Lee, H.J. (2007) Rapid formation for hyperpycnal sediment gravity currents offshore of a semi-arid California river. *Continental Shelf Research* 28, 991-1009.

Wolbach, W.S., Lewis, R.S., Anders, E. (1985) Cretaceous extinctions; Evidence for wildfires and search for meteoritic material. *Science* 230, 167-170.

Wolbach, W.S., Anders, E., Nazarov., M.A. (1990a) Fires at the K/T boundary: Carbon at the Sumbar, Turkmenia, site. *Geochimica et Cosmochimica Acta* 54, 1133-1146.

Wolbach, W.S., Gilmour, I., Anders, E. (1990b) Major wildfires at the K-T boundary. In: Sharpton, V.L., Ward, P.D. (Eds.) *Global Catastrophes in Earth History*. GSA Special Paper, Boulder, CO, 247, 391-400.

Woolley, R.R. (1946) Cloudburst floods in Utah 1850-1938. *U.S. Geological Survey, W.S. Paper* 994, 1-128.

Wright, J.D., Schaller, M.F. (2013) Evidence for a rapid release of carbon at the Paleocene-Eocene thermal maximum. *PNAS* 110, 15908-15913.

Zeebe, R.E., Ridgwell, A., Zachos, J.C. (2016) Anthropogenic carbon release rate unprecedented during the past 66 million years. *Nature Geoscience* 9, 325-329.